20

### Visualization of Fluorescence Lifetime Decay in Single Cells for Evaluating the Biocompatibility of Self-Assembling Hydrogels

© T.N. Tikhonova<sup>1</sup>, A.M. Mozherov<sup>2</sup>, A.V. Barkovaya<sup>1</sup>, Yu.M. Efremov<sup>2</sup>, D.S. Kuznetsova<sup>2</sup>, P.S. Timashev<sup>2,3</sup>, V.I. Shcheslavskiy<sup>4</sup>, V.V. Fadeev<sup>1</sup>, B.P. Yakimov<sup>1,2</sup>¶

e-mail: tikhonova@physics.msu.ru, ¶bp.jakimov@physics.msu.ru

Received January 22, 2025 Revised January 31, 2025 Accepted April 07, 2025

Hydrogels self-assembled from short peptides are garnering significant interest due to their remarkable mechanical and biological properties, making them promising for applications in tissue engineering, regenerative medicine, 3D cell culture, and drug delivery. One of the key challenges in developing hydrogels with different structures and chemical compositions is to carefully evaluate their biocompatibility with cells, including the ability of cells to survive, proliferate, and differentiate inside hydrogels. One method for assessing cell viability is fluorescence lifetime imaging microscopy (FLIM), which allows for the detection of changes in cellular metabolism via the signal of endogenous fluorophores at the single-cell level. In this study, the potential for assessing changes in cellular metabolism was investigated using human breast cancer cells (MCF-7) cultured on soft, self-organizing hydrogels with varying levels of biocompatibility made from Fmoc-FF peptide and chitosan. It was demonstrated that FLIM data, combined with advanced segmentation methods based on universal zero-shot Segment Anything neural network model, can assess the metabolic status of cells at the single-cell level in large sample sizes. The presented method enables the tracking of metabolic changes in cells adhered to soft hydrogels and the early detection of scaffold biocompatibility with tissue cells, which is promising for regenerative technology applications.

Keywords: hydrogel, fluorescence lifetime imaging microscopy, cell, metabolism.

DOI: 10.61011/EOS.2025.05.61649.28-25

#### Introduction

The study of the characteristics of cells adhered to hydrogels is an important element of regenerative medicine [1–5]. Understanding the interaction of cells with the environment plays a key role in creating new biomaterials, improving tissue engineering techniques, and developing more efficient drug delivery systems. Currently, there is an increasing interest in hydrogels based on the Fmoc-FF peptide in regenerative medicine [6–8]. These hydrogels, consisting of self-assembling peptide nanofibers, represent promising platforms for cell culture due to their unique characteristics [9,10]. The softness of the Fmoc-FF hydrogel contributes to the accurate reproduction of the mechanical properties of natural tissues, which makes it attractive for various applications in the field of tissue engineering.

One of the key problems that arise when creating new hydrogels for the tasks of regenerative technologies is a fast, accurate and reliable assessment of cell viability on artificial tissue-engineered structures, which does not require additional manipulations with the sample. Fluorescence lifetime imaging microscopy (FLIM) of cells and tissues has proven to be a powerful tool in biological research due to the ability to study the morphological and biophysical details of the studied structures, as well as due to its

Cellular components can be labeled low invasiveness. using specific dyes and the functionality of individual organelles can be studied, however, many cells themselves contain endogenous fluorophores that can be used to obtain information about cellular metabolism [11-14]. One of the endogenous tissue fluorophores is nicotinamide adenine dinucleotide (NAD). Being an important cofactor in cellular respiration, NAD plays a significant role in energy production and metabolic pathways and is found in cells in reduced (NADH), oxidized (NAD+) and phosphorylated forms (NAD(P)H or NADP+). NADH and NAD(P)H are autofluorescent among them, while NADH exhibits the highest fluorescence intensity in cells [15]. These pigments which are present in free form (e.g., in the cytoplasm) or bound to proteins (e.g., in mitochondria) exhibit a characteristic lifetime, indicating their involvement in glycolysis or oxidative phosphorylation. Fluorescence lifetime NAD(P)H is an important parameter for distinguishing between these two forms. Free NAD(P)H usually has a shorter fluorescence lifetime, approximately 0.4 ns, while protein-bound NAD(P)H has a longer lifetime, usually in the range from 1.8 to 5.7 ns, reflecting its interaction with various cellular proteins [16]. FLIM allows quantifying the distribution and dynamics of free and bound NAD(P)H in cells, which can improve the understanding of cellular

<sup>&</sup>lt;sup>1</sup> Lomonosov Moscow State University, Faculty of Physics, Moscow, Russia

<sup>&</sup>lt;sup>2</sup> Institute for Regenerative Medicine, Sechenov University, Moscow, Russia

<sup>&</sup>lt;sup>3</sup> Moscow State University named after M.V. Lomonosov, Faculty of Chemistry, Moscow, Russia

<sup>&</sup>lt;sup>4</sup> Research Institute of Experimental Oncology and Biomedical Technologies, Nizhny Novgorod, Russia

metabolism and its regulation under various physiological and pathological conditions [17–19].

When assessing the metabolic status using the FLIM method, it is important to assess the status by individual single cells, rather than by a macroscopic section of tissue, since even closely located cellular subpopulations can exhibit metabolic heterogeneity [20]. At the same time, manually selecting related image areas belonging to individual cells is a laborious procedure. For example, up to several hundred individual cells can be present in a single image. Taking into account the fact that several dozens or even hundreds of images are typically measured to verify reproducibility and various effects on the attenuation parameters of the fluorescent response, manual segmentation of single cells becomes a "bottleneck" in the analysis of experimental FLIM data.

For automatic segmentation of single cells in microscopy images, including FLIM images, various neural network architectures can be used, which assign to each pixel of the image a label corresponding to a single cell or background [20,21]. However, in most cases, this approach also requires a pre-assembled large set of training data with known segmented areas on which the model must be trained. The so-called "zero-shot" approach (transfer without additional training) is one of the approaches to avoid labelling the data and training the model before applying it. Zero-shot models are pre-trained on a wide and heterogeneous dataset for semantic segmentation tasks so that the model has high segmentation quality on images that are not similar to those presented in the training dataset. The Segment Anything Model (SAM) has been one of the most popular zero-shot models in the last two years [22,23], which shows high quality in both household photographs and medical images [24]. At the same time, this model was not used to analyze FLIM images in order to analyze single cells.

This paper demonstrates the possibility of using the FLIM method with endogenous fluorescent contrast NAD(P)H to analyze the metabolism of MCF-7 cells during their interaction with tissue-engineered structures from self-assembling short peptide Fmoc-FF and hydrogel from a mixture of Fmoc-FF with the addition of chitosan. We demonstrate that the FLIM method makes it possible to detect changes in the metabolic status of cells during its interaction with the hydrogel, while the method of estimating parameters for single cells using the approach we developed using the zero-shot SAM model for FLIM image segmentation is more sensitive. The presented method makes it possible to identify and monitor changes in the metabolism of cells adhered to soft hydrogels, and at an early stage to identify the biocompatibility of scaffolds with tissue cells, which is promising for the tasks of regenerative technologies.

#### Materials and methods

#### 1.1. Preparation of samples

Reagents. The peptide N-fluorenylmethoxycarbonyldiphenylalanine (Fmoc-Phe-Phe-OH, Fmoc-FF) was purchased from Sigma-Aldrich (USA), and dulbecco's modified eagle medium (DMEM) was purchased from Gibco (USA).

Hydrogels. The Fmoc-FF hydrogel was prepared by changing the solvent. Solvent change hydrogels were prepared as follows: peptides were dissolved in dimethyl sulfoxide (DMSO) to obtain a starting solution,  $C_{\text{Fmoc-FF}}$ (starting) = 10%, then the starting solution was dissolved in mQ-water to the final concentration  $C_{\rm Fmoc-FF} = 0.6 \%$ . After the preparation of the hydrogels, they were thoroughly washed with a solution of PBS buffer for 2 days to ensure complete removal of DMSO [15] (for the solvent change method), as well as to achieve a hydrogel pH of 7.3 instead of pH of 4. Fmoc-FF hydrogels with the addition of low molecular weight chitosan (Fmoc-FF + chitosan) (M = 190 kDa) were prepared as follows: peptides were dissolved in DMSO to obtain the initial solution,  $C_{\text{Fmoc-FF}}$  (initial) = 10%, chitosan was dissolved in HCl(1 M),  $C_{chitosan}$  (initial) = 1%. Chitosan was added to the water to a final concentration of 0.6%,  $C_{\text{chitosan}}$ (final) = 0.06%, after which the initial solution  $F_{\text{moc-FF}}$  was mixed with it so as to obtain  $C_{\text{Fmoc-FF}}$  (final) = 0.6%, so  $C_{\rm Fmoc\text{-}FF}/C_{\rm chitosan}=10:1.$  The hydrogel was washed for several hours with PBS buffer to obtain a final hydrogel pH of 7.3.

Cell culture. MCF-7 breast cancer cell lines were grown in a complete DMEM culture medium (PanEco, Russia) containing 10% serum (FBS) (Gibco, USA), 1x PenStrep (Gibco, USA) and 1x GlutaMAX (Gibco, USA) in a standard culture incubator with 5% CO<sub>2</sub> at a temperature of 37°C. The cells were seeded on gels formed on confocal plates in an amount of 300,000 per cup and incubated at 37°C, 5% CO<sub>2</sub> for 24 h. Cells seeded on gel-free confocal cups were used as controls.

## 1.2. Microscopy of fluorescence lifetime visualization

The images of the intensity and lifetime of fluorescence of NAD(P)H in monolayer cell cultures were acquired using NikonTi2-U microscope with a FLIM module: SPC-180NX TCSPC (Becker& Hickl GmbH, Germany), GaAsP hybrid photodetector for photon counting 300–720 nm HPM-100-40 (Becker& Hickl GmbH, Germany). The CFI Apochromat LWD Lambda S 40XC WI NA = 1.15 immersion lens was used for imaging. Two-photon fluorescence was excited by a femtosecond Ti,;,Sa laser Toptica Femto Fiber Ultra (repetition frequency 80 MHz, pulse duration 140 fs) at a wavelength of 780 nm and it was recorded in the range of 420–470nm. The average power applied to the samples was 5–10 mW. The approximate photon counting rate was

 $(1\!-\!2)\cdot 10^5$  photons per second. The signal accumulation time was  $120\,s.$  The measurements were carried out at room temperature.

The fluorescence attenuation curves on the obtained FLIM images were processed pixel-by-pixel using a twoexponential attenuation model taking into account convolution with a Gaussian detector response function. The signal-noise ratio was increased by spatial averaging of the attenuation curves over the area of  $11 \times 11$  pixels ("binning" = 5). The attenuation time of the short component  $\tau_1$  was fixed to 400 ps to reduce the number of free parameters. The free approximation parameters were: the long lifetime component  $\tau_2$ , the amplitudes of the short-lived and long-lived components  $\alpha_1$  and  $\alpha_2$ , respectively. The average fluorescence attenuation time  $(\tau_m = (\alpha_1 \tau_1 + \alpha_2 \tau_2)/(\alpha_1 + \alpha_2))$  and the ratio of component amplitudes  $\alpha_1/\alpha_2$  were calculated as an additional "integral" parameter. The approximation quality,  $\chi_2$ , was in the range of 0.8-1.2. The FLIM images were processed using the SPCImage 8.6 software (Becker& Hickl GmbH, Germany).

## 1.3. Automatic segmentation of single cells in FLIM images

The following procedure was used to automatically select cells in FLIM images. Maps of the intensity of the fluorescence response — the integral number of photons detected under the fluorescence attenuation curve in each pixel of the image — with a size of  $512 \times 512$  pixels were used for the analysis. All intensity values were limited in the first step from the bottom to the quantile value of 0.01 and from the top to the quantile value of 0.99 for eliminating extremely high and extremely low intensity values. After that, to eliminate the heterogeneity of the intensity distribution, the image was contrasted using the adaptive histogram equalization algorithm with a core of  $64 \times 64$  pixels and was fed to the input of the SAM model (ViT-L version) [25], operating in the "Everything" mode, i.e. returning all possible objects that the model recognized in the image.

After obtaining masks of individual objects, the segmented areas were selected by area and image intensity: areas with an average intensity value of more than 10% of the maximum intensity level in the image were selected by intensity; areas with a size of more than 300 and less than 1000 pixels were selected by area. The average values of the fluorescence attenuation parameters over the region were calculated for the specified segmentation regions such as amplitudes  $\alpha_1$  and  $\alpha_2$ , attenuation times  $\tau_1$  and  $\tau_2$ , average attenuation time were calculated  $\tau_m$  and amplitude ratios  $\alpha_1/\alpha_2$ . In total, 5 images for the control group, 8 images obtained for cells cultured on Fmoc-FF hydrogel, and 7 images of cells obtained for cells cultured on a hydrogel made of Fmoc-FF and chitosan were analyzed using this method. The sample consisted of 386 cells of

the control group, 826 cells of the "Fmoc-FF" group, 245 cells of the "Fmoc-FF+ chitosan" group.

#### 1.4. Statistical data analysis

The fluorescence response attenuation parameters were compared using the Kraskell statistical criterion using the Bonferroni correction for multiple comparisons. Data processing and statistical analysis were performed using software scripts implemented in Python3 using Pandas, Scipy, Matplotlib, Pytorch, and Sam libraries.

#### 2. Results

# 2.1. Pixel-by-pixel assessment of changes in the metabolism of MCF-7 cells adhered to the soft hydrogel Fmoc-FF

To study the metabolism of cells during their adhesion to a hydrogel, the initially self-assembling hydrogel Fmoc-FF was formed on a Petri dish using the solvent change method (sec. 1). The hydrogel Fmoc-FF is a soft polymer characterized by a fibrillar structure and high water content (70–95%) [26]. After that, the cells were incubated on it and examined using FLIM. As a result of the measurements, a map of the average fluorescence attenuation time was constructed, from which it was possible to obtain the average lifetime, as well as other parameters of fluorescence attenuation of the regions corresponding to single cells (Fig.1).

Fig. 2 shows optical images of MCF-7 cells placed on a Petri dish (control) (Fig. 2, a), on the hydrogel Fmoc-FF (Fig. 2, b) and on hydrogel Fmoc-FF + chitosan (fig. 2, c). Chitosan, a polysaccharide derived from natural chitin, is attracting attention in the field of tissue engineering due to its ability to increase cell viability, biocompatibility, and biodegradability [27,28].

According to maps of the average fluorescence attenuation time for cells placed on the control (Fig. 2, d), on the hydrogel Fmoc-FF (Fig. 2, e) and on the hydrogel Fmoc-FF+, chitosan (Fig. 2, f), it can be seen that the metabolism of cells under control and the Fmoc-FF hydrogel is different, while the addition of chitosan to the hydrogel leads to the cell-on-hydrogel system becoming more similar in its characteristics to the control. A pixel-by-pixel comparison of fluorescence attenuation kinetics for all studied systems showed that for cells located on a Petri dish, the average lifetime  $\tau_{\rm m(control)}=1410\,{\rm ps}$  is longer than the lifetime for cells located on the hydrogel Fmoc-FF and the hydrogel Fmoc-FF+chitosan,  $\tau_{\rm m(Fmoc-FF)}=1190\,{\rm ps}$  and  $\tau_{\rm m(Fmoc-FF+chitosan)}=1240\,{\rm ps}$ , respectively.

As noted earlier, the short component  $(\alpha_1)$  of NAD(P) fluorescence corresponds to the free form NAD(P)H, and the long component corresponds to the form bound to the protein  $(\alpha_2)$ . Decrease in the average lifetime of NAD(P)H fluorescence in case of the cells adhesion to a soft hydrogel Fmoc-FF is associated with an increase

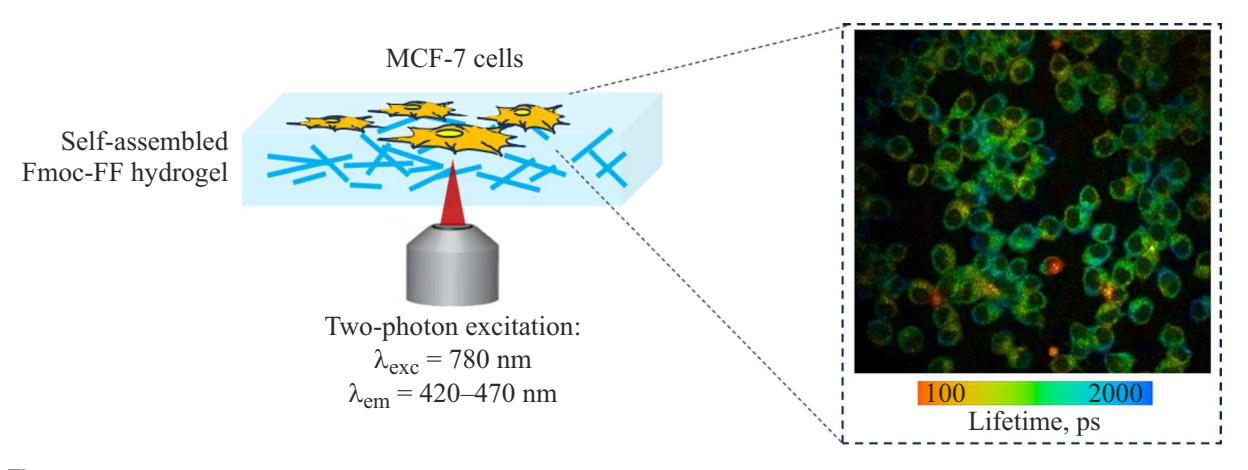
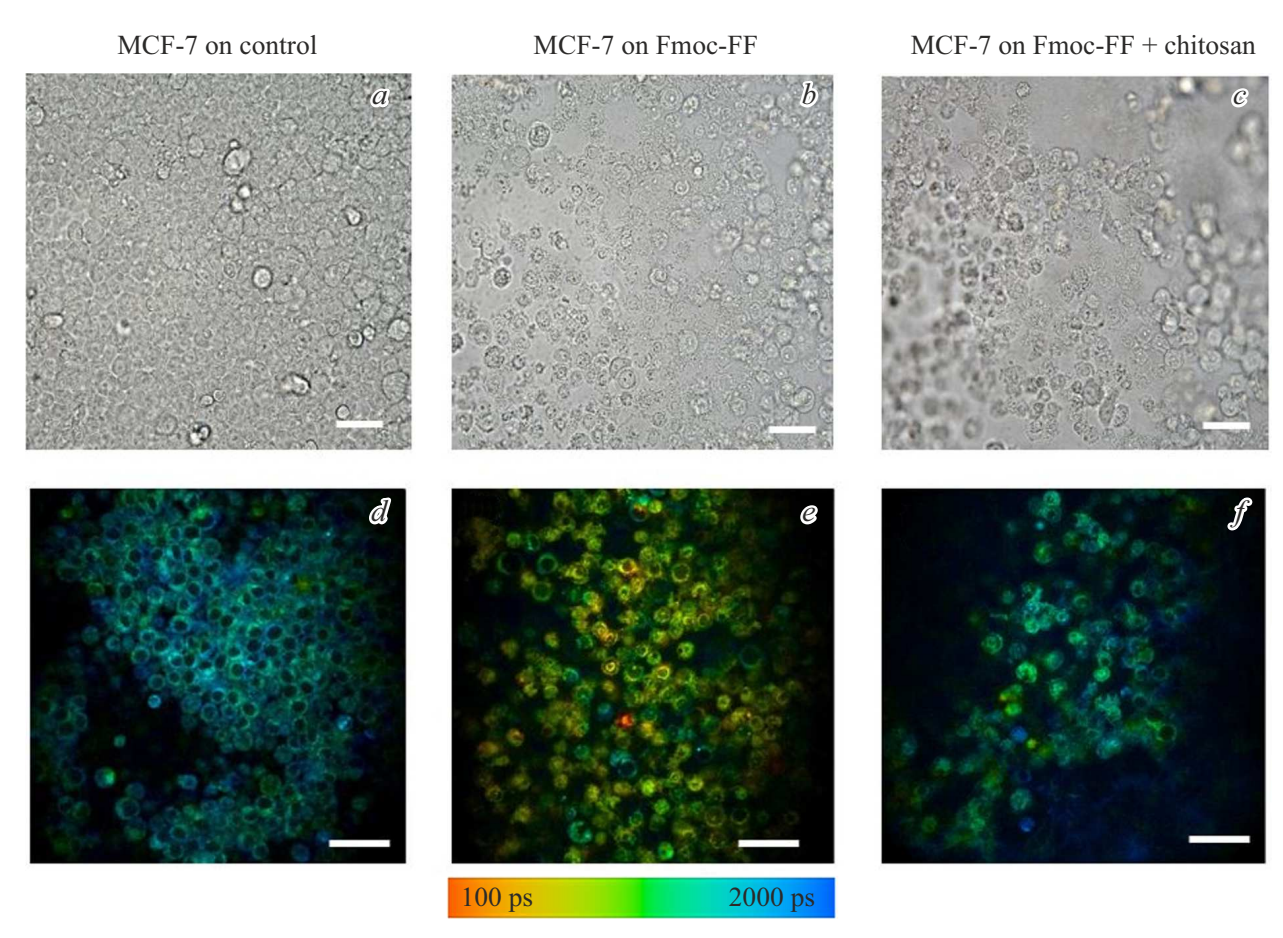


Figure 1. Scheme of the experiment to study the metabolism of living cells adhered to a hydrogel using the FLIM method.



**Figure 2.** Optical images of MCF-7 cells placed on a (a) Petri dish (control), (b) hydrogel Fmoc-FF, (c) hydrogel Fmoc-FF+chitosan. Average fluorescence attenuation maps for MCF-7 cells placed on (d) control, (e) on the hydrogel Fmoc-FF and (f) for the hydrogel Fmoc-FF+chitosan. Scale marker  $45 \, \mu \text{m}$ .

in the contribution of the free form  $\alpha_1$  from 63 to 68, while the lifetime of the free component  $\tau_1$  decreases from 600 to 430 ps. Such a change may indicate that in cells placed on a hydrogel, anaerobic glycolysis begins to make a greater contribution to metabolism, which may lead to a deterioration in cell survival on such hydrogels

compared with the control [17–19]. The reasons for such changes may be changes in the mechanical properties of the substrates, as well as their chemical composition. The addition of chitosan to hydrogels leads to an increase in the average lifetime  $\tau_{m(Fmoc\text{-}FF+chitosan)}=1240\,\mathrm{ps}$ , which correlates with the ability of chitosan to increase

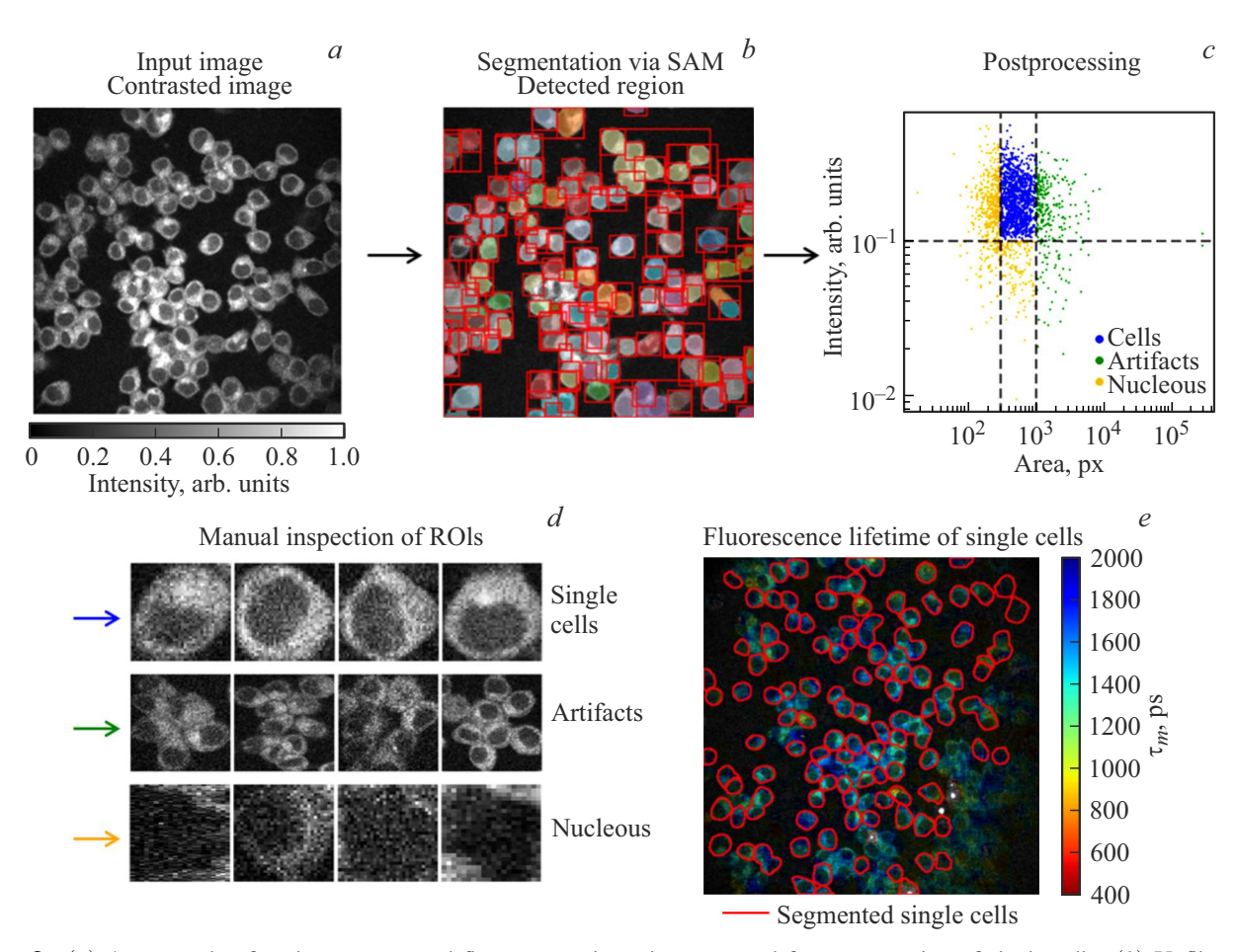


Figure 3. (a) An example of an input contrasted fluorescence intensity map used for segmentation of single cells. (b) Unfiltered cell segmentation results obtained using SAM; separate segmentation areas are highlighted with red rectangles (separate fill colors in the image). (c) The distribution of the area of the segmented areas and the average fluorescence intensity in the corresponding areas; dashed lines define the zones separating the areas of cells (blue dots) from the area of separately segmented cell nuclei (green dots) and other artifacts (orange dots). (d) Examples of areas of segmented cells, artifacts, and individual nuclei. (e) An example of superimposing the boundaries of segmented regions (red lines) with a map of the average fluorescence attenuation time.

cell viability and improve the biocompatibility of hydrogels [27,28].

#### 2.2. Automatic segmentation of single cells in FLIM images using zero-shot models

As can be seen, the changes in the average lifetime, as well as the changes of other parameters of fluorescence attenuation (amplitudes and times  $\tau_1$  and  $\tau_2$ ) of regions corresponding to single cells are observed on the maps of the average fluorescence attenuation time. However, a pixel-by-pixel comparison of fluorescence attenuation maps is not correct when analyzing cell images — the determined fluorescence attenuation parameters may be influenced by the background fluorescence response, the contribution of "cellular debris" and other artifacts. Cell-by-cell analysis is more correct and more sensitive in the analysis, in which attenuation parameters are analyzed, averaged over the regions corresponding to single cells.

In this paper, we have developed and tested a method using the zero-shot Segment Anything Model (SAM) to segment single cells in an image. The application of the method is described in detail in Sect. 1.3. briefly point out that the input images were images of fluorescence intensity, filtered so as to eliminate bright and dark artifacts in the images and eliminate the inhomogeneity of illumination (Fig. 3, a). The images were segmented using the SAM architecture, which assigned to each pixel a label corresponding to one or more objects in the image.

It was found that most of the cells are segmented in this way in the FLIM input images, however, segmentation artifacts are present (Fig. 3, b): the model highlighted areas corresponding to several cells, the model separately highlighted the nuclei, highlighted parts of the background. In order to eliminate these markup artifacts, the following postprocessing procedure was applied for segmentation results (Fig. 3, c): it was assumed that cells are areas with an area of 300 to 1000 pixels and an average intensity of at

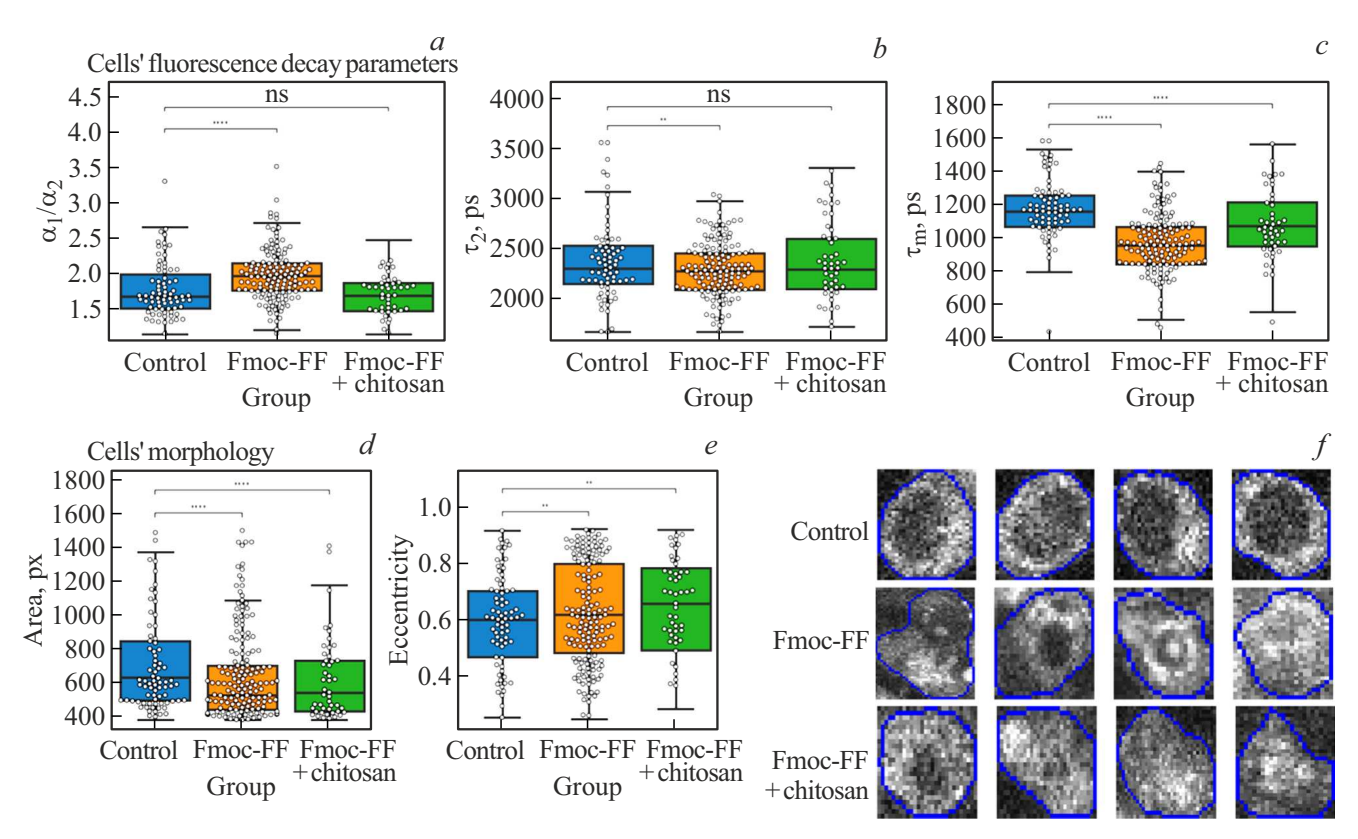


**Figure 4.** Distribution of parameters (a) of the ratio of the amplitudes of the fast and slow components  $\alpha_1/\alpha_2$ , (b) attenuation time  $\tau_2$ , (c) average time  $\tau_m$ , (d) squares and (e) eccentricity of the segmentation mask for MCF-7 cells on the Petri dish (control) (blue columns), on the Fmoc-FF hydrogel (orange columns) and MCF-7 on the Fmoc-FF+chitosan hydrogel (green columns). (f) Typical examples of segmented cells of the control groups, Fmoc-FF and "Fmoc-FF+chitosan".

least 10% of the maximum intensity in the image. Indeed, visual inspection showed that most of the cells belong to this area of segmentation parameters (Fig. 3, d).

Examples of segmentation regions on fluorescence attenuation maps are shown in Fig. 3, e. In total, 5 images for the control group, 8 images obtained for cells cultured on Fmoc-FF hydrogel, and 7 images of cells obtained for cells cultured on a hydrogel made of Fmoc-FF and chitosan were analyzed using the proposed method. For each segmented region, the average values of the fluorescence attenuation parameters were calculated, which were then used for statistical analysis.

#### 2.3. Analysis of fluorescence attenuation parameters of single cells in the presence of self-assembling hydrogels

Using the developed segmentation method, a sample of fluorescence attenuation parameters was obtained for 386 cells of the control group, 826 cells of the "group" Fmoc-FF, 245 cells of the "group Fmoc-FF+ chitosan". The distribution of the ratio of the amplitudes of the fast and slow components  $\alpha_1/\alpha_2$ , the attenuation time  $\tau_2$ , and the average attenuation time  $\tau_m$  are shown in Fig. 4, a–with. As can be seen, in comparison with the control for

cells planted on Fmoc-FF, there is a significant change in the fluorescence attenuation parameters: the ratio of the amplitudes of the components  $\alpha_1/\alpha_2$  increases from 1.70 to 1.98  $(p < 10^{-4})$ , the median attenuation time of the long-lived component  $\tau_2$ , associated with a bound NAD(P)H, weakly however statistically significantly decreases from 2310 to 2270 ps  $(p < 10^{-2})$ , which leads to a decrease in the average attenuation time  $\tau_{\text{m}}$  from 1160 to 950 ps  $(p < 10^{-4})$ . The addition of chitosan to the Fmoc-FF hydrogel has a much less pronounced effect on changes in fluorescence attenuation parameters. Thus, unlike the Fmoc-FF cell group, there is no statistically significant shift in the median value of the amplitude ratio  $\alpha_1/\alpha_2$  and the lifetime of the long-lived component  $\tau_2$ (p > 0.05), however, the median average attenuation time is statistically significantly lower — 1080 ps for the group "Fmoc-FF + chitosan" vs. 1160 ps in the control group  $(p < 10^{-4})$ . The observed shifts indicate a significant effect of the hydrogel from Fmoc-FF on the metabolic activity of cells. The addition of chitosan to the hydrogel from Fmoc-FF leads to fewer changes in the parameters of FLIM. At the same time, it turns out that the most sensitive parameter for assessing changes in metabolic status is the average fluorescence decay time  $\tau_{\rm m}$  — when comparing the control groups and "Fmoc-FF+chitosan"

statistically significant differences are observed only in this parameter. The data obtained correlate with the dynamics of changes in fluorescence attenuation parameters, revealed by pixel-by-pixel comparison of fluorescence attenuation maps for the studied samples, while allowing tracking changes in parameters at the level of single cells.

Simultaneously with changes in the parameters of fluorescence attenuation, cell-by-cell segmentation makes it possible to evaluate changes in cell morphology. Fig. 4, d, e shows the area and eccentricity distributions for cell segmentation regions obtained using the segmentation algorithm. The eccentricity characterizes the "elongation" of the cell, the zero value corresponds to the shape of the segmentation mask close to a circle, while the eccentricity close to one corresponds to cells significantly elongated along a certain direction. As can be seen, in the case of control sample cells cultured without the addition of hydrogel, the cells occupied a larger area in the analyzed images and had a more rounded shape. At the same time, in the presence of hydrogel, cell morphology significantly changed — cells decreased in area  $(p < 10^{-2})$ , while the value of eccentricity ( $p < 10^{-2}$ ) changed. Typical examples of single cells of each group are shown in Fig. 4, f. It should be noted that in addition to changes in cell area and eccentricity values, the cells visually differed in the ratio of the areas occupied by the cell nucleus and cytoplasm (Fig. 4, f)Such visual differences in morphology can also be used to assess cell status when testing various hydrogels for biocompatibility.

#### Conclusion

The noninvasive FLIM method with endogenous fluorescent contrast over (F) was used in this work to study the metabolism of living MCF-7 cells in case of their adhesion to self-assembling hydrogels Fmoc-FF and Fmoc-FF,+,chitosan, which can serve as potential scaffolds in the field of regenerative medicine. This method demonstrated that cell survival decreases for cells adhered to the Fmoc-FF hydrogel, which can be explained by the processes of transition from aerobic to anaerobic glycolysis when the substrate changes. The addition of chitosan to the hydrogel leads to an increase in the biocompatibility of the scaffold. This paper shows that the method of estimating parameters for single cells using the developed approach using the zero-shot SAM model for FLIM image segmentation makes it possible to more accurately assess the metabolic status of cells compared with the data obtained by pixel-by-pixel comparison of fluorescence attenuation maps for the studied samples. The performed procedure can be adapted to study any cell-soft hydrogel system in order to identify the most biocompatible soft hydrogel for use in regenerative medicine.

#### Funding

This study was financially supported by the Russian Science Foundation (grant No.23-75-00007).

#### References

- Z. Liu, M. Tang, J. Zhao, R. Chai, J. Kang. Adv. Mater., 30 (17), 1705388 (2018). DOI: 10.1002/adma.201705388
- [2] S. Pina, V.P. Ribeiro, C.F. Marques, F.R. Maia, T.H. Silva,
   R.L. Reis, J.M. Oliveira. Mater., 12 (11), 1824 (2019).
   DOI: 10.3390/ma12111824
- [3] Y. Tang, H. Wang, S. Liu, L. Pu, X. Hu, J. Ding, G. Xu, W. Xu, S. Xiang, Z. Yuan. Colloids Surf. B, 220, 112973 (2022). DOI: 10.1016/j.colsurfb.2022.112973
- [4] Y. Liang, J. He, B. Guo. ACS Nano, 15 (8), 12687 (2021). DOI: 10.1021/acsnano.1c04206
- [5] B.C. Borro, R. Nordstr?m, M. Malmsten. Colloids Surf. B, 187, 110835 (2020). DOI: 10.1016/j.colsurfb.2020.110835
- [6] V. Basavalingappa, T. Guterman, Y. Tang, S. Nir, J. Lei, P. Chakraborty, L. Schnaider, M. Reches, G. Wei, E. Gazit. Adv. Sci., 6 (12), 1900218 (2019). DOI: 10.1002/advs.201900218
- [7] C. Diaferia, M. Ghosh, T. Sibillano, E. Gallo, M. Stornaiuolo, C. Giannini, G. Morelli, L. Adler-Abramovich, A. Accardo. Soft Matter., 15 (3), 487 (2019). DOI: 10.1039/C8SM02366B
- [8] M. Vitale, C. Ligorio, B. McAvan, N.W. Hodson, C. Allan, S.M. Richardson, J.A. Hoyland, J. Bella. Acta Biomater., 138, 144 (2022). DOI: 10.1016/j.actbio.2021.11.011
- [9] T.N. Tikhonova, V.S. Kolmogorov, R.V. Timoshenko, A.N. Vaneev, D. Cohen-Gerassi, L.A. Osminkina, P.V. Gorelkin, A.S. Erofeev, N.N. Sysoev, L. Adler-Abramovich, E.A. Shirshin. Cells, 11 (24), 4137 (2022).
  DOI: 10.3390/cells11244137
- [10] T.N. Tikhonova, D. Cohen-Gerassi, Z.A. Arnon, Y. Efremov, P. Timashev, L. Adler-Abramovich, E.A. Shirshin. ACS Appl. Mater. Interfaces, 14 (50), 55392 (2022). DOI: 10.1021/acsami.2c17609
- [11] K. Suhling, L.M. Hirvonen, J.A. Levitt, P.H. Chung, C. Tregidgo, A. Le Marois, D.A. Rusakov, K. Zheng, S. Ameer-Beg, S. Poland, S. Coelh, R. Henderson, N. Krstajic. Med. Photonics, 27, 3 (2015). DOI: 10.1016/j.medpho.2014.12.001
- [12] S.R. Alam, H. Wallrabe, Z. Svindrych, A.K. Chaudhary, K.G. Christopher, D. Chandra, A. Periasamy. Sci. Rep., 7 (1), 10451 (2017). DOI: 10.1038/s41598-017-10856-3
- [13] S. Kalinina, C. Freymueller, N. Naskar, B. von Einem, K. Reess, R. Sroka, A. Rueck. Int. J. Mol. Sci., 22 (11), 5952 (2021). DOI: 10.3390/ijms22115952
- [14] M.C. Skala, K.M. Riching, A. Gendron-Fitzpatrick, J. Eickhoff, K.W. Eliceiri, J.G. White, N. Ramanujam. Proc. Natl. Acad. Sci., 104 (49), 19494 (2007). DOI: 10.1073/pnas.0708425104
- [15] O.I. Kolenc, K.P. Quinn. Antioxid. Redox Signal., 30 (6), 875 (2019). DOI: 10.1089/ars.2017.7451
- [16] K. Blinova, S. Carroll, S. Bose, A.V. Smirnov, J.J. Harvey, J.R. Knutson, R.S. Balaban. Biochemistry, 44 (7), 2585 (2005). DOI: 10.1021/bi0485124
- [17] D.K. Bird, L. Yan, K.M. Vrotsos, K.W. Eliceiri, E.M. Vaughan,
   P.J. Keely, J.G. White, N. Ramanujam. Cancer Res., 65 (19),
   8766 (2005). DOI: 10.1158/0008-5472.CAN-04-3922

- [18] E. Stuntz, Y. Gong, D. Sood, V. Liaudanskaya, D. Pouli, K.P. Quinn, C. Alonzo, Z. Liu, D.L. Kaplan, I. Georgakoudi. Sci. Rep., 7 (1), 1041 (2017). DOI: 10.1038/s41598-017-01015-9
- [19] J.M. Berthiaume, J.G. Kurdys, D.M. Muntean, M.G. Rosca. Antioxid. Redox Signal., 30 (3), 375 (2019). DOI: 10.1089/ars.2017.7415
- [20] E.A. Shirshin, M.V. Shirmanova, A.V. Gayer, M.M. Lukina, E.E. Nikonova, B.P. Yakimov, G.S. Budylin, V.V. Dudenkova, N.I. Ignatova, D.V. Komarov, V.V. Yakovlev, W. Becker, E.V. Zagaynova, V.I. Shcheslavskiy, M.O. Scully. Proc. Natl. Acad. Sci., 119 (9), e2118241119 (2022). DOI: 10.1073/pnas.2118241119
- [21] T. Vicar, J. Balvan, J. Jaros, F. Jug, R. Kolar, M. Masarik, J. Gumulec. BMC Bioinformatics, 20, 1 (2019). DOI: 10.1186/s12859-019-2880-8
- [22] A. Kirillov, E. Mintun, N. Ravi, H. Mao, C. Rolland, L. Gustafson, T. Xiao, S. Whitehead, A.C. Berg, W.-Y. Lo, P. Dollar, R. Girshick. Proc. IEEE/CVF Int. Conf. Comput. Vis., 4015–4026 (2023).
- [23] N. Ravi, V. Gabeur, Y.-T. Hu, R. Hu, C. Ryali, T. Ma, H. Khedr, R. Rädle, C. Rolland, L. Gustafson, E. Mintun, J. Pan, K.V. Alwala, N. Carion, C.-Y. Wu, R. Girshick, P. Dollár, C. Feichtenhofer. arXiv preprint arXiv:2408.00714 (2024). DOI: 10.48550/arXiv.2408.00714
- [24] Y. Huang, X. Yang, L. Liu, H. Zhou, A. Chang, X. Zhou, R. Chen, J. Yu, J. Chen, C. Chen, S. Liu, H. Chi, X. Hu, K. Yue, L. Li, V. Grau, D.-P. Fan, F. Dong, D. Ni. Med. Image Anal., 92, 103061 (2024). DOI: 10.1016/j.media.2023.103061
- [25] URL: https://github.com/facebookresearch/segment-anything
- [26] C. Diaferia, G. Morelli, A. Accardo. J. Mater. Chem. B, 7 (34), 5142 (2019). DOI: 10.1039/C9TB01043B
- [27] M. Boido, M. Ghibaudi, P. Gentile, E. Favaro, R. Fusaro,
   C. Tonda-Turo. Sci. Rep., 9 (1), 6402 (2019).
   DOI: 10.1038/s41598-019-42848-w
- [28] T.T. Demirtaş, G. Irmak, M. Gümüşderelioğlu. Biofabrication, 9 (3), 035003 (2017). DOI: 10.1088/1758-5090/aa7b1d

Translated by A.Akhtyamov